

Universality of quantum phase transitions in the integer and fractional quantum Hall regimes

Received: 6 May 2024

Accepted: 24 September 2024

Published online: 02 October 2024

 Check for updatesSimrandeep Kaur^{1,8}, Tanima Chanda^{1,8}, Kazi Rafsanjani Amin^{2,8}, Divya Sahani¹, Kenji Watanabe³, Takashi Taniguchi⁴, Unmesh Ghorai⁵, Yuval Gefen⁶, G. J. Sreejith⁷ & Aveek Bid¹✉

Fractional quantum Hall (FQH) phases emerge due to strong electronic interactions and are characterized by anyonic quasiparticles, each distinguished by unique topological parameters, fractional charge, and statistics. In contrast, the integer quantum Hall (IQH) effects can be understood from the band topology of non-interacting electrons. We report a surprising super-universality of the critical behavior across all FQH and IQH transitions. Contrary to the anticipated state-dependent critical exponents, our findings reveal the same critical scaling exponent $\kappa = 0.41 \pm 0.02$ and localization length exponent $\gamma = 2.4 \pm 0.2$ for fractional and integer quantum Hall transitions. From these, we extract the value of the dynamical exponent $z \approx 1$. We have achieved this in ultra-high mobility trilayer graphene devices with a metallic screening layer close to the conduction channels. The observation of these global critical exponents across various quantum Hall phase transitions was masked in previous studies by significant sample-to-sample variation in the measured values of κ in conventional semiconductor heterostructures, where long-range correlated disorder dominates. We show that the robust scaling exponents are valid in the limit of short-range disorder correlations.

The quantum Hall (QH) effect, observed in a two-dimensional electron gas subject to a perpendicular magnetic field, realizes multiple quantum phase transitions (QPT) between distinct insulating topological states¹. The magnetic field \mathbf{B} quenches the electronic kinetic energy into disorder-broadened discrete Landau energy levels (LL). All electronic single-particle states are localized, barring those at a specific critical energy E_c near the center of each LL, which are extended²⁻⁷. When the Fermi energy lies between the extended states of two successive LLs, the system is in a distinct topological phase characterized by a quantized value of Hall resistance R_{xy} and vanishingly small

longitudinal resistance R_{xx} . As the Fermi energy approaches E_c , the localization length ξ characterizing the single-particle states diverges as $\xi \sim |E - E_c|^{-\gamma}$ while the slowest time-scale diverges as $\tau \sim \xi^z \sim |E - E_c|^{-z\gamma}$ ^{8,9}. The exponent γ governs the critical divergence of the localization length as the filling fraction or magnetic field approach the critical values and z governs the divergence of the coherence length with decreasing temperatures¹⁰. From the finite-size scaling theory^{10,11},

$$dR_{xy}/d\nu_{\nu_c} \propto T^{-1/z\gamma} \quad (1)$$

¹Department of Physics, Indian Institute of Science, Bangalore 560012, India. ²Department of Microtechnology and Nanoscience, Chalmers University of Technology, 412 96 Gothenburg, Sweden. ³Research Center for Electronic and Optical Materials, National Institute for Materials Science, 1-1 Namiki, Tsukuba 305-0044, Japan. ⁴Research Center for Materials Nanoarchitectonics, National Institute for Materials Science, 1-1 Namiki, Tsukuba 305-0044, Japan. ⁵Department of Theoretical Physics, Tata Institute of Fundamental Research, Homi Bhabha Road, Mumbai 400005, India. ⁶Department of Condensed Matter Physics, Weizmann Institute of Science, Rehovot 76100, Israel. ⁷Indian Institute of Science Education and Research, Pune 411008, India. ⁸These authors contributed equally: Simrandeep Kaur, Tanima Chanda, Kazi Rafsanjani Amin. ✉e-mail: aveek@iisc.ac.in

Here, $\nu = nh/eB$, n is the areal charge-carrier density, h is the Planck constant, e is the electronic charge, and T is the temperature. One additionally defines the scaling exponent $\kappa = 1/z\gamma^{1-13}$ that governs this temperature dependence of the slope of R_{xy} as well as the width of the R_{xx} peak at the transition. The values of these three critical exponents (of which only two are independent) have been argued to be universal, with $\gamma \approx 2.3$, $\kappa \approx 0.42$, and $z = 1$ for all IQH transitions^{4,10,11,14,15}.

Low temperatures and high magnetic fields enhance the effective electron-electron interactions, producing a richer set of the fractional quantum Hall (FQH) phases at rational filling fractions¹⁶. The question then arises: Can IQH and FQH phase transitions be analyzed using a ‘unified’ scaling framework¹⁷? While the IQH phases originate from the topology of the single particle electronic Chern bands¹⁸, the FQH phases are crucially underlain by strong electronic interactions. These are marked by distinct electronic correlations, topological order, ground state degeneracy, and topological entanglement. The transition between FQH plateaus is driven by a proliferation of anyonic quasiparticles (characterized by quasiparticle statistics and fractional charge). This picture may suggest that the critical behavior at the transitions depends on the specifics of the topological FQH states involved and is also different from the analogous transitions in the IQH regime.

Experimental investigations of scaling in the IQH regime have reported κ varying between $0.16 \leq \kappa \leq 0.81$ (Supplementary Information, Supplementary Note 13). This wide variation has been attributed to varying disorder correlation lengths with a universal critical behavior seen only in samples with short-range disorder^{19,20}. This lack of a tight constraint on κ has hindered any claims of their universality. Similar experimental investigations of scaling laws at transitions between FQH phases are scarce^{21–23}. A recent experimental study on extremely high-mobility 2D electron gas confined to GaAs quantum wells found the value of κ in the FQH regime to be non-universal, this observation being attributable to long-range disorder correlation²³. Thus, despite over three decades of study, the fundamental question of the values of the critical exponents across quantum Hall transitions (integer and fractional) remains unsettled^{14,23,24}.

This article reports the experimental observation of a surprising super universality in the scaling exponents for transitions between various IQH and FQH phases in trilayer graphene. We measure both the scaling exponent κ and the localization length exponent γ independently over several integer-to-integer, integer-to-fractional, and fractional-to-fractional Quantum Hall transitions. Contrary to the

expected picture of multiple plateau-to-plateau quantum phase transitions, each with its own distinct critical properties, here we find that for all IQH and FQH plateau-to-plateau transitions (PT), $\kappa = 0.41 \pm 0.02$, $\gamma \approx 2.4 \pm 0.2$, and $z \approx 1$, closely aligned with the predictions of the scaling theory of localization¹³. Given the distinct origins of the two phenomena, this striking similarity of the critical exponents suggests a connection between the IQH and FQH effects that transcends the composite fermion (CF) framework.

We estimate the values of κ near criticality ($\nu \approx \nu_c$) using three distinct approaches: (i) analyzing the critical divergence of $dR_{xy}/d\nu$, (ii) probing the critical divergence of the inverse width of $R_{xx}(T)$, and (iii) a scaling analysis of R_{xy} near the critical point. The localization exponent γ is obtained deep in the tails of the localized regime from the dependence of G_{xx} on ν . A scaling analysis of Quantum Hall transitions for fractional and integer states provides a second, independent way to extract γ .

The realizations of these quantum phase transitions in graphene-based systems are associated with a highly tunable set of parameters. These include the ability to alter electron density, which is typically unachievable in semiconductor heterostructures²⁵, the capability to manage screening, and the option to induce band mixing by applying a displacement field \mathbf{D} . This flexibility helps us establish that weak Landau level mixing does not significantly affect these critical exponents.

Graphene also provides a platform where the nature of disorder scattering can be controlled. This is because the electrical transport properties of high-mobility graphene devices are dominated by short-range impurity scattering, while those of low-mobility graphene devices are controlled by both short-ranged and long-ranged scattering potentials^{26,27}. Thus, high-mobility graphene devices represent a natural candidate to investigate the universality of scaling exponents. Our comparative study between graphene devices of varying mobility shows that as long as long-range impurity scattering can be suppressed, the universality of scaling parameters persists, independent of the quantum Hall bulk phases involved.

Results

Standard dry transfer technique is used for the fabrication of dual graphite-gated hexagonal-boron-nitride (hBN) encapsulated TLG devices (Fig. 1a) (for details, see Supplementary Information, Supplementary Note 1)²⁸. Figure 1b shows measurements of the longitudinal resistance R_{xx} and the transverse conductance G_{xy} versus the Landau level filling factor ν ; the measurements were performed at $\mathbf{B} = 13$ T,

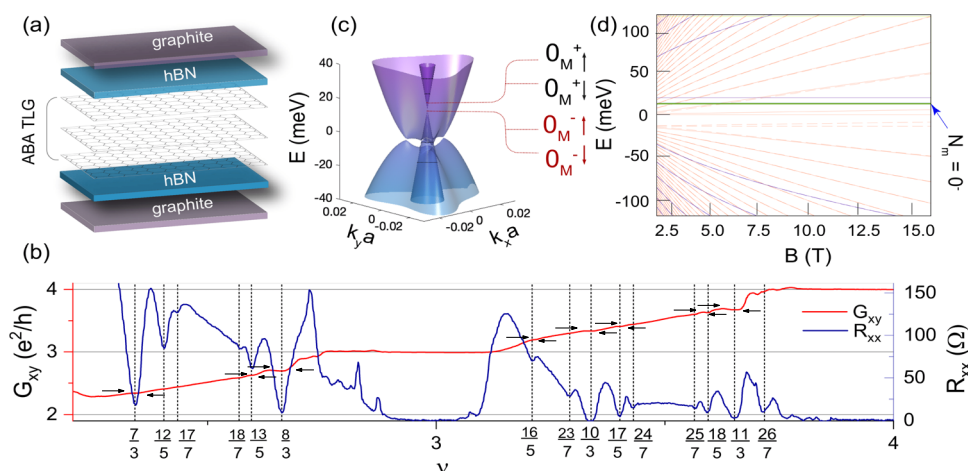


Fig. 1 | FQH in Bernal-stacked TLG. **a** Device schematic of TLG encapsulated between two hBN and few-layer graphite flakes. **b** Line plots of G_{xy} (left-axis; solid red line) and R_{xx} (right-axis; solid blue line) versus ν measured at $\mathbf{B} = 13$ T, $T = 20$ mK, and $\mathbf{D} = 0$ V/nm. The dashed vertical lines mark the FQH states formed at corresponding ν , and the arrows indicate corresponding plateaus in G_{xy} . **c** Calculated band structure of Bernal stacked trilayer graphene for $\mathbf{D} = 0$ V/nm. The four LLs of the $N_M = 0$ (The

MLG LLs are marked by the subscripts M , and orbital contents are given by the numbers O) band are indicated schematically. **d** Calculated Landau levels as a function of energy E and \mathbf{B} for $\mathbf{D} = 0$ V/nm. The blue lines are the monolayer-like LLs, while the red lines are the bilayer-like LLs. The solid and dotted lines indicate the LLs from K and K' -valley, respectively. The solid-green line is the spin-degenerate $N_M = 0 \uparrow$ and $N_M = 0 \downarrow$ monolayer-like LLs that host the FQH states probed in this article.

$T = 20$ mK, and $\mathbf{D} = 0$ V/nm. We identify several major odd denominator FQH states by prominent dips in R_{xx} and corresponding plateaus in G_{xy} . Indications of developing $\nu = 3 + 1/5$ and $3 + 2/7$ states are also seen. Several of these FQH states are resolved at $\mathbf{B} = 4.5$ T, attesting to the high quality of the device in terms of excellent homogeneity of number density and suppression of long-range scattering (Supplementary Information, Supplementary Note 6).

The band structure of TLG is formed of monolayer-like and bilayer-like Landau levels (Fig. 1c)—these are protected from mixing by the lattice mirror-symmetry²⁹. The calculated LL spectrum as a function of \mathbf{B} and energy E is shown in Fig. 1d, where blue (red) lines mark the monolayer-like (bilayer-like) LLs. For $\mathbf{B} > 8$ T, the $\nu = 2$ and $\nu = 3$ arise from the spin-split $N_M = 0^{\uparrow}$ and $N_M = 0^{\downarrow}$ bands of the monolayer-like LLs. Here, (+, -) refers to the two valleys, and (\uparrow , \downarrow) refers to electronic spins. We confine our study to $8 \text{ T} < \mathbf{B} < 13 \text{ T}$ to avoid Landau level-mixing at lower \mathbf{B} and phase transitions between competing FQH states at higher \mathbf{B} ^{30–32}.

Critical exponents near FQH plateau-to-plateau transitions

Figure 2a shows the T -dependence of R_{xy} between the IQH states $\nu = -2$ and $\nu = -1$. Similar data for transition between the FQH states $\nu = 2 + 2/3$ and $\nu = 2 + 3/5$ are shown in Fig. 2b. The critical points ν_c of the plateau-to-plateau transition (identified as the crossing point of the R_{xy} curves at different T) are indicated in the plots. The exponent κ evaluated from the peak value of $dR_{xy}/d\nu$ versus T near criticality (Fig. 2c and d) in both cases is $\kappa = 0.41 \pm 0.01$. Analysis of the T -dependence of the inverse of the half-width of R_{xx} as ν is varied between two consecutive FQH plateaus also yields $\kappa = 0.41 \pm 0.02$ (Supplementary Information, Supplementary Note 2).

To demonstrate the scaling properties of R_{xy} in the vicinity of ν_c , we use the following form¹³:

$$R_{xy}(\nu, T) = R_{xy}(\nu_c) f[\alpha(\nu - \nu_c)] \quad (2)$$

with $\alpha \propto T^\kappa$. Here, $f(0) = 1$, and $f'(0) \neq 0$. This gives us a third, independent method of estimating κ . Figure 2e shows the plots of $R_{xy}/R_{xy}(\nu_c)$ at various temperatures as a function of $\alpha|\nu - \nu_c|$ for the $\nu = 2 + 1/3$ to $2 + 2/5$ transition. $\alpha(T)$ is optimized to collapse the various constant-temperature data onto a single curve (the upper branch of which is for $\nu < \nu_c$ and the lower branch is for $\nu > \nu_c$). From the plot of α versus T (inset of Fig. 2e) we obtain $\kappa = 0.40 \pm 0.03$.

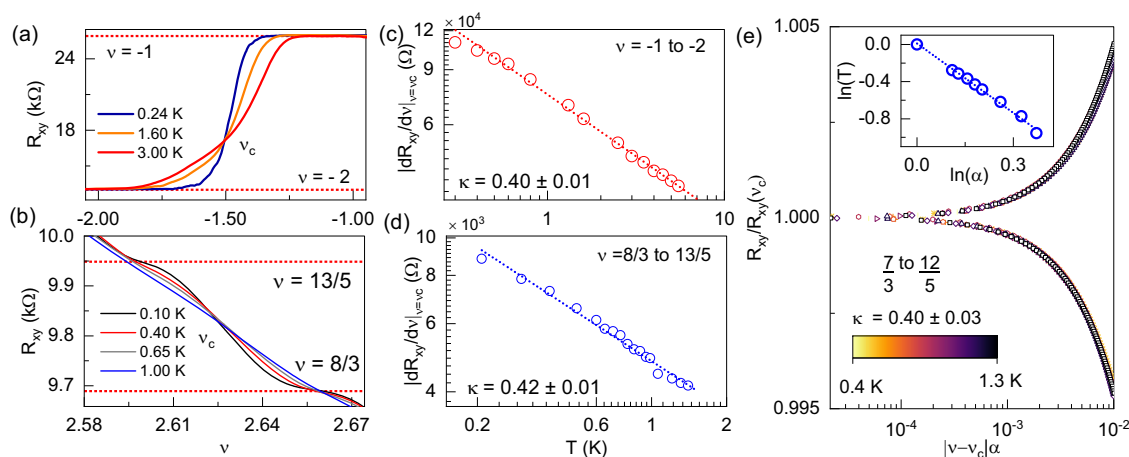


Fig. 2 | Scaling near $\nu = \nu_c$. Plot of R_{xy} versus ν for transition between the (a) IQH states $\nu = -2$ and $\nu = -1$ (the critical point $\nu_c = -1.5$) and (b) the FQH states $2 + 2/3$ and $2 + 3/5$ ($\nu_c = 2.625$). c Double logarithmic plot of $|dR_{xy}/d\nu|_{\nu=\nu_c}$ versus T for the PT $\nu = -2$ and $\nu = -1$ at ν_c . The dashed line is the fit to the data points using Eq. (1). d Same as in (c) for the PT

To check the validity of our scaling analysis, we perform the following error analysis: The residue in the least square fit between the scaling curves (like those shown in Fig. 2e) for each assumed value of κ is calculated. This quantity, which we call 'fit error', is presented in Supplementary Information Supplementary Fig. 6 and Supplementary Fig. 7 in a semi-log scale; we find that the fit error is indeed minimum for $\kappa = 0.41$.

Figure 3a compiles our findings. These results indicate a κ value of 0.41 ± 0.03 uniformly observed across all probed transitions between IQH and FQH states (compare with Supplementary Fig. 14 of Supplementary Information). This consistency in scaling exponents spans various transition types, including (1) transitions from one IQH state to another, (2) transitions among different FQH states, and (3) transitions between an IQH state and a neighboring FQH state. It is important to emphasize that the observed universality of κ goes beyond marking an experimental confirmation of a uniform scaling law across FQH transitions in any material. Given the distinct physics of IQH and FQH states, such constancy of the scaling exponent is remarkable and underscores the universal applicability of the scaling principle across QH transitions. This is the central result of this article.

Locating the transition

The physics of the FQH effect of electrons at a filling factor ν can be mapped onto that of IQH of CF at a filling factor ν_{CF} , with $\nu = \nu_{CF}/(2\nu_{CF} \pm 1)$ ³³. It follows that the critical points for the transition between successive FQH phases at $\nu = \nu_{CF}/(2\nu_{CF} \pm 1)$ and $\nu = (\nu_{CF} + 1)/(2(\nu_{CF} + 1) \pm 1)$ occur at^{14,34}:

$$\nu_c = \frac{(\nu_{CF} + 0.5)}{2(\nu_{CF} + 0.5) \pm 1} \quad (3)$$

The experimentally obtained values of ν_c , extracted either from the crossing point of the R_{xy} isotherms or the maxima of R_{xx} , match exceptionally well with the theoretical predictions (Fig. 3b) (Supplementary Information, Supplementary Table 1).

Robustness of the critical exponents against LL mixing

A non-zero vertical displacement field \mathbf{D} gives rise to a complex phase diagram in TLG, with the Landau levels inter-crossing multiple times, resulting in significant LL mixing as either \mathbf{D} or \mathbf{B} is varied^{35–39}. LL-mixing can change the effective interaction between the electrons³². However, as shown in Fig. 3c, it does not significantly affect the

between FQH states $2 + 2/3$ and $2 + 3/5$. e Scaling analysis of R_{xy} for the PT transition between $\nu = 2 + 1/3$ and $\nu = 2 + 2/5$. The inset is a plot of T versus α in a double logarithmic scale (open circles); a linear fit to the data (dotted line) yields $\kappa = 0.40 \pm 0.03$. (For an error analysis, see Supplementary Information, Supplementary Note 7).

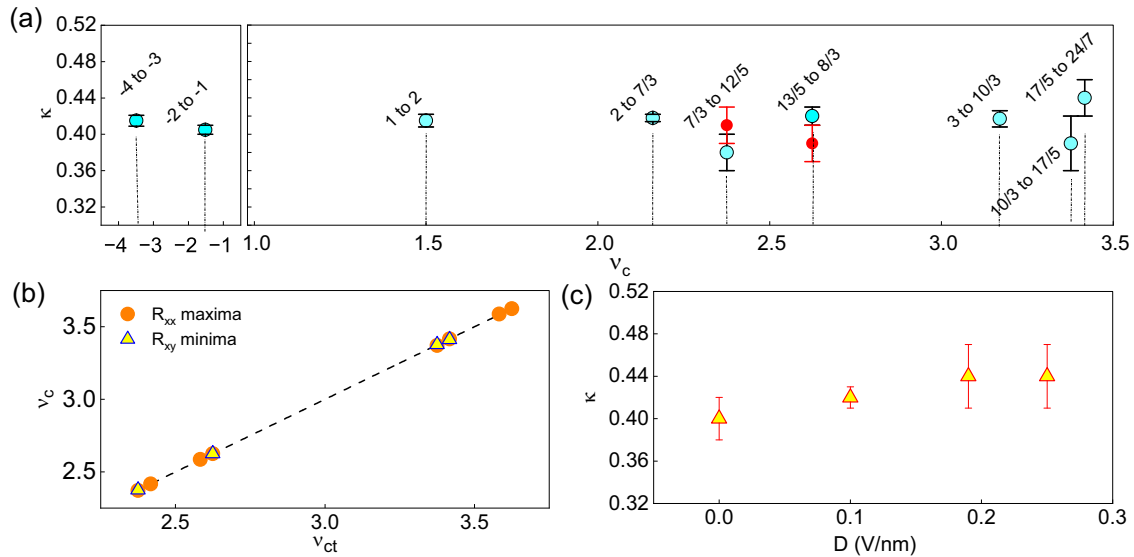


Fig. 3 | Scaling exponents for different PT. **a** Plot of κ as a function of ν_c corresponding to different PT evaluated from the maxima of derivative $(dR_{xy}/d\nu)^{\max}$ near the critical point. The dotted vertical lines mark the experimentally obtained ν_c . The light blue symbols are for the κ values obtained for trilayer graphene, and the red symbols are for the single-layer graphene. **b** Plot of experimentally obtained values of critical points, ν_c versus those theoretically calculated ν_{ct} ¹⁴. The triangles

are the values determined from crossing points of isotherms in R_{xy} , while the circles are determined from the R_{xx} maxima. The black dashed line fits the data points with slope = 1.00 ± 0.002 . **c** Plot of κ versus D for the FQH transition from $\nu = 8/3$ to $\nu = 13/5$ states evaluated from the maxima of derivative $(dR_{xy}/d\nu)^{\max}$ near the critical point. The error bars are determined from the least-square fits to the data.

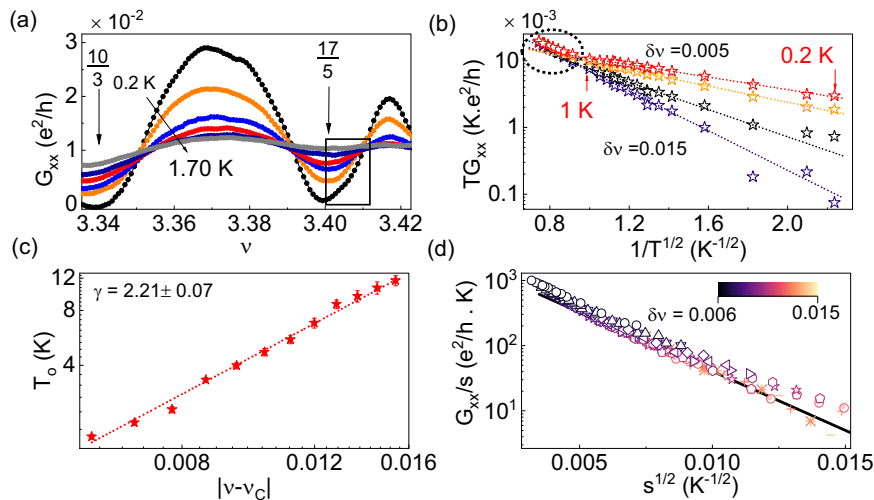


Fig. 4 | Scaling exponent in the ES regime for $\nu = 3 + 2/5$ to $3 + 3/7$ transition. **a** Plots of the T -dependence of G_{xx} versus filling factor ν for two FQH states between $\nu = 3$ and $\nu = 4$. The black box marks the region where the ES analysis was carried out. **b** Fit of ES Eq. (4) (dotted lines) to the G_{xx} data for the transition from $\nu = 3 + 2/5$ and $\nu = 3 + 3/7$. Each set of data points is for a given value of $\delta\nu = |\nu - \nu_c|$ with $\nu_c = 3.416$. The plots deviate from the expected ES behavior at high T (the region is marked

with an ellipse). **c** Plots of T_0 versus $\delta\nu_{CF}$. The dotted line is a linear fit to the data (see Eq. (5)). The slope yields the value of γ . The error bars are determined from the least square fits to the data in (b). **d** Plot of scaled longitudinal conductance G_{xx}/s as a function of scaling parameter $s = |\delta\nu|/T$ for PT between $\nu = 17/5$ and $\nu = 24/7$. The scatter points of different colors are for different values of $|\delta\nu|$, and the solid black line is fit to Eq. (6).

universality of κ . This vital result suggests that as long as the anyons are weakly interacting, the critical behavior of the localization-delocalization transition remains unaltered.

Measurement of localization exponent γ

We now focus on the localized regime, far away from E_c , marked by the black rectangle in Fig. 4a. Given the presence of strong interactions, it is reasonable to assume that transport in this localized part of the energy spectrum proceeds through Efros–Shklovskii (ES) type hopping mechanism⁴⁰. The localization exponent γ determines the T

dependence of longitudinal conductance G_{xx} ^{40,41}:

$$G_{xx} = G_0 e^{-(T_0/T)^{1/2}} \tag{4}$$

with

$$k_B T_0 \propto |\delta\nu|^\gamma. \tag{5}$$

The pre-factor $G_0 \propto 1/T$ and $\delta\nu = (\nu - \nu_c)$. Figure 4b shows plots of $\log(TG_{xx})$ versus $T^{-1/2}$ at different values of $\delta\nu$; the dotted lines are linear

fits to the data. The linearity of the data at low- T is consistent with transport by the ES hopping mechanism in the FQH regime (Eq. (4)). At high- T (in the region marked in Fig. 4b by a dotted ellipse), the values of G_{xx} become relatively large, and the plots deviate from a straight line. In passing, we note that as we move progressively closer to the center of the plateau in R_{xy} , where the value of $G_{xx} \approx 0$ at low- T , the linearity of the plots persists to higher temperatures. Fitting T_0 (estimated from Eqn (4)) and $|\delta v_{CF}|$ to Eq. (5), we find the estimated γ to lie in the range 2.3–2.6 (Fig. 4c) for FQH plateau-to-plateau transitions, very close to the predicted range of $\gamma = 2.3$ – 2.5^{14} . The fact that the exponent controlling the divergence of the localization length at criticality is almost identical for both FQH and IQH states points to an effective model of localization that is universal across the different statistics of the quasiparticles in these QH phases. Furthermore, from $\kappa = 1/z\gamma \approx 0.41 \pm 0.03$ and $\gamma \approx 2.3$, we get $z \approx 1$, as expected for a strongly interacting system^{7,9,42,43}.

An independent estimate of γ is obtained by casting Eq. (4) into a single-parameter scaling form⁴⁴:

$$G_{xx}(s) = \sigma^* s e^{-(T^*s)^{1/2}}, \quad (6)$$

with the scaling parameter $s = |\delta v_{CF}|/T$. Figure 4d shows the scaling plots of G_{xx}/s versus $s^{1/2}$ for the PT in ES regime from $\nu = 3 + 2/5$ to $\nu = 3 + 3/7$. We find a near-perfect data collapse for all values of δv_{CF} in the localized regime with $\gamma \approx 2.3$, providing an independent validation of the universality of γ .

Discussion

We are now in a position to compare the universality of κ seen in the FQH PT in our high-mobility TLG with non-universality of the same measured in the high-mobility 2D semiconductors²³. The large spread in the observed values of κ seen in the data in GaAs quantum wells was attributed to two main reasons²³. The first is the formation of numerous emerging FQH phases between $\nu = 1/3$ and $2/5$, which limits the temperature range over which one observes the decrease of the width of R_{xx} with T . Note that in Fig. 1b, there are two incipient FQH phases, $\nu = 3 + 1/5$ and $3 + 2/7$, between the more robust phases $\nu = 3$ and $\nu = 3 + 1/3$. The incipient phases are weak enough not to affect the scaling of the transition region in R_{xy} even at the lowest temperature employed here. As a result, we find $\kappa = 0.42 \pm 0.01$ (Fig. 3a).

The second reason is related to the type of disorder in the sample²³. Universality in κ is observed only when the effective disorder potential is short-ranged²⁰, as in our graphite-gated high-mobility graphene devices. This is not the case in GaAs/AlGaAs systems, where long-range scattering potential from the impurities cannot be ignored²³. We fabricated graphene devices without the graphite gate electrodes to probe the effect of long-range interactions on κ . The graphene channel was no longer screened from long-range Coulomb fluctuations arising from the SiO₂ substrate; this was reflected in reduced mobility ~ 2 – 5 m²/Vs. While in these devices, we do not find FQH states, the value of κ for IQH transitions varied widely between 0.45–0.64 (Supplementary Information, Supplementary Note 4), supporting the conclusions of ref. 23.

To summarize, our principal finding is that scaling properties for transitions involving Abelian FQH states and/or IQH phases are universal. Specifically, we have demonstrated the scaling of the longitudinal conductance (with a scaling exponent $\kappa = 0.41 \pm 0.02$ and localization exponent $\gamma \approx 2.3$) in the IQH and FQH states in Bernal-stacked ABA trilayer graphene. This conclusion holds for plateau-to-plateau transitions between two consecutive IQH states, two FQH states, and even between IQH and the adjoining FQH state, underlining the universal character of the scaling. This universality of κ persists even when an external displacement field hybridizes the Landau levels of Bernal-stacked TLG. In fact, we find deviations from universality in

the value of κ only in devices where long-range scattering dominates. To our knowledge, ours is the first definite scaling analysis of the QPT over a series of fractional QH states.

FQH phases are underlined by strongly correlated and interacting electrons. Our results demonstrate a surprising correspondence between the FQH phase transitions and those of non-interacting electrons. The results indicate a super-universality in the localization–delocalization transitions across distinct anyonic species that represent the characteristic quasiparticles of the FQH phases. While much is known about the localization of electrons, the observed super universality motivates the study of localization in anyonic quasiparticles and the mechanism that drives their conduction in the presence of disorder and quasiparticle interactions. Our study raises the natural question of whether the universality observed in this context applies to transitions between other topological phases with fractional excitations, such as fractional Chern insulators⁴⁵.

Methods

Device fabrication

Devices of dual graphite gated ABA trilayer graphene (TLG) heterostructures were fabricated using a dry transfer technique (for details, see Supplementary Information Supplementary Note 1). Raman spectroscopy and optical contrast were used to determine the number of layers and the stacking sequence. The devices were patterned using electron beam lithography followed by reactive ion etching and thermal deposition of Cr/Pd/Au contacts. Dual electrostatic gates were used to simultaneously tune the areal number density $n = [(C_{tg}V_{tg} + C_{bg}V_{bg})/e + n_o]$ and the displacement field $D = [(C_{bg}V_{bg} - C_{tg}V_{tg})/2\epsilon_0 + D_o]$ across the device. Here C_{bg} (C_{tg}) is the capacitance of the back gate (top gate), and V_{bg} (V_{tg}) is the voltage of the back gate (top gate). The values of C_{tg} and C_{bg} are determined from quantum Hall measurements. n_o and D_o are the residual number density and electric field due to unavoidable impurities in the channel.

Transport measurements

The electrical transport measurements were performed in a dilution refrigerator (with a base temperature of 20 mK) at low frequency (11.4 Hz) using standard low-frequency measurement techniques, with a bias current of 10 nA.

Data availability

The authors declare that the data supporting the findings of this study are available within the main text and its Supplementary Information and at <https://doi.org/10.6084/m9.figshare.26809147.v1>. Other relevant data are available from the corresponding author upon request.

Code availability

The codes that support the findings of this study are available from the corresponding author upon request.

References

1. Klitzing, K. V., Dorda, G. & Pepper, M. New method for high-accuracy determination of the fine-structure constant based on quantized hall resistance. *Phys. Rev. Lett.* **45**, 494–497 (1980).
2. Huo, Y. & Bhatt, R. N. Current carrying states in the lowest Landau level. *Phys. Rev. Lett.* **68**, 1375–1378 (1992).
3. Laughlin, R. B. Quantized hall conductivity in two dimensions. *Phys. Rev. B* **23**, 5632–5633 (1981).
4. Aoki, H. & Ando, T. Critical localization in two-dimensional Landau quantization. *Phys. Rev. Lett.* **54**, 831–834 (1985).
5. Chalker, J. T. & Daniell, G. J. Scaling, diffusion, and the integer quantized hall effect. *Phys. Rev. Lett.* **61**, 593–596 (1988).
6. Chalker, J. T. & Coddington, P. D. Percolation, quantum tunnelling and the integer hall effect. *J. Phys. C: Solid State Phys.* **21**, 2665 (1988).

7. Huckestein, B. & Backhaus, M. Integer quantum hall effect of interacting electrons: Dynamical scaling and critical conductivity. *Phys. Rev. Lett.* **82**, 5100–5103 (1999).
8. Halperin, B. I. & Hohenberg, P. C. Scaling laws for dynamic critical phenomena. *Phys. Rev.* **177**, 952–971 (1969).
9. Li, W. et al. Scaling in plateau-to-plateau transition: a direct connection of quantum Hall systems with the Anderson localization model. *Phys. Rev. Lett.* **102**, 216801 (2009).
10. Sondhi, S. L., Girvin, S. M., Carini, J. P. & Shahar, D. Continuous quantum phase transitions. *Rev. Mod. Phys.* **69**, 315–333 (1997).
11. Pruisken, A. M. M. Universal singularities in the integral quantum hall effect. *Phys. Rev. Lett.* **61**, 1297–1300 (1988).
12. Doodoo-Amoo, N. A. et al. Non-universality of scaling exponents in quantum hall transitions. *J. Phys.: Condens. Matter* **26**, 475801 (2014).
13. Huckestein, B. Scaling theory of the integer quantum hall effect. *Rev. Mod. Phys.* **67**, 357–396 (1995).
14. Pu, S., Sreejith, G. J. & Jain, J. K. Anderson localization in the fractional quantum hall effect. *Phys. Rev. Lett.* **128**, 116801 (2022).
15. Huckestein, B. & Kramer, B. One-parameter scaling in the lowest Landau band: Precise determination of the critical behavior of the localization length. *Phys. Rev. Lett.* **64**, 1437–1440 (1990).
16. Tsui, D. C., Stormer, H. L. & Gossard, A. C. Two-dimensional magnetotransport in the extreme quantum limit. *Phys. Rev. Lett.* **48**, 1559–1562 (1982).
17. Hohenberg, P. C. & Halperin, B. I. Theory of dynamic critical phenomena. *Rev. Mod. Phys.* **49**, 435–479 (1977).
18. Thouless, D. J., Kohmoto, M., Nightingale, M. P. & den Nijs, M. Quantized Hall conductance in a two-dimensional periodic potential. *Phys. Rev. Lett.* **49**, 405–408 (1982).
19. Wei, H. P., Lin, S. Y., Tsui, D. C. & Pruisken, A. M. M. Effect of long-range potential fluctuations on scaling in the integer quantum hall effect. *Phys. Rev. B* **45**, 3926–3928 (1992).
20. Li, W., Csáthy, G. A., Tsui, D. C., Pfeiffer, L. N. & West, K. W. Scaling and universality of integer quantum hall plateau-to-plateau transitions. *Phys. Rev. Lett.* **94**, 206807 (2005).
21. Engel, L., Wei, H. P., Tsui, D. C. & Shayegan, M. Critical exponent in the fractional quantum hall effect. *Surf. Sci.* **229**, 13–15 (1990).
22. Machida, T., Ishizuka, S., Komiyama, S., Muraki, K. & Hirayama, Y. Scaling in fractional quantum hall transitions. *Phys. B: Condens. Matter* **298**, 182–186 (2001).
23. Madathil, P. T. et al. Delocalization and universality of the fractional quantum hall plateau-to-plateau transitions. *Phys. Rev. Lett.* **130**, 226503 (2023).
24. Kumar, P., Nosov, P. A. & Raghu, S. Interaction effects on quantum hall transitions: dynamical scaling laws and superuniversality. *Phys. Rev. Res.* **4**, 033146 (2022).
25. Pan, W. et al. Particle-hole symmetry and the fractional quantum hall effect in the lowest Landau level. *Phys. Rev. Lett.* **124**, 156801 (2020).
26. Sarkar, S. et al. Role of different scattering mechanisms on the temperature dependence of transport in graphene. *Sci. Rep.* **5**, 16772– (2015).
27. Rhodes, D., Chae, SangHoon, Ribeiro-Palau, R. & Hone, J. Disorder in van der Waals heterostructures of 2d materials. *Nat. Mater.* **18**, 541–549 (2019).
28. Pizzocchero, F. et al. The hot pick-up technique for batch assembly of van der Waals heterostructures. *Nat. Commun.* **7**, 11894 (2016).
29. Koshino, M. & McCann, E. Landau level spectra and the quantum Hall effect of multilayer graphene. *Phys. Rev. B* **83**, 165443 (2011).
30. Papić, Z., Abanin, D. A., Barlas, Y. & Bhatt, R. N. Tunable interactions and phase transitions in Dirac materials in a magnetic field. *Phys. Rev. B* **84**, 241306 (2011).
31. Zhu, Z., Sheng, D. N. & Sodemann, I. Widely tunable quantum phase transition from moore-read to composite Fermi liquid in bilayer graphene. *Phys. Rev. Lett.* **124**, 097604 (2020).
32. Sodemann, I. & MacDonald, A. H. Landau level mixing and the fractional quantum Hall effect. *Phys. Rev. B* **87**, 245425 (2013).
33. Jain, J. K. Composite-fermion approach for the fractional quantum hall effect. *Phys. Rev. Lett.* **63**, 199–202 (1989).
34. Goldman, V. J., Jain, J. K. & Shayegan, M. Nature of the extended states in the fractional quantum hall effect. *Phys. Rev. Lett.* **65**, 907–910 (1990).
35. Zibrov, A. A. et al. Emergent Dirac gullies and gully-symmetry-breaking quantum hall states in a b a trilayer graphene. *Phys. Rev. Lett.* **121**, 167601 (2018).
36. Rao, P. & Serbyn, M. Gully quantum Hall ferromagnetism in biased trilayer graphene. *Phys. Rev. B* **101**, 245411 (2020).
37. Winterer, F. et al. Spontaneous gully-polarized quantum hall states in aba trilayer graphene. *Nano Lett.* **22**, 3317–3322 (2022).
38. Serbyn, M. & Abanin, D. A. New Dirac points and multiple Landau level crossings in biased trilayer graphene. *Phys. Rev. B* **87**, 115422 (2013).
39. Wang, Yun-Peng, Li, Xiang-Guo, Fry, J. N. & Cheng, Hai-Ping First-principles studies of electric field effects on the electronic structure of trilayer graphene. *Phys. Rev. B* **94**, 165428 (2016).
40. Efros, A. L. & Shklovskii, B. I. Coulomb gap and low temperature conductivity of disordered systems. *J. Phys. C: Solid State Phys.* **8**, L49 (1975).
41. Ono, Y. Localization of electrons under strong magnetic fields in a two-dimensional system. *J. Phys. Soc. Jpn.* **51**, 237–243 (1982).
42. Hohls, F. et al. Dynamical scaling of the quantum Hall plateau transition. *Phys. Rev. Lett.* **89**, 276801 (2002).
43. Polyakov, D. G. & Shklovskii, B. I. Conductivity-peak broadening in the quantum Hall regime. *Phys. Rev. B* **48**, 11167–11175 (1993).
44. Hohls, F., Zeitler, U. & Haug, R. J. Hopping conductivity in the quantum Hall effect: revival of universal scaling. *Phys. Rev. Lett.* **88**, 036802 (2002).
45. Han, T. et al. Correlated insulator and Chern insulators in pentalayer rhombohedral-stacked graphene. *Nat. Nanotechnol.* **19**, 181–187 (2024).

Acknowledgements

We thank Jainendra K. Jain, Sankar Das Sarma, Rajdeep Sensarma, Nandini Trivedi, Ravindra Bhatt and Prasant Kumar for helpful discussions and clarifications. We acknowledge Ramya Nagarajan for data on low-mobility samples. A.B. acknowledges funding from U.S. Army DEVCOM Indo-Pacific (Project number: FA5209 22PO166) and Department of Science and Technology, Govt of India (DST/SJF/PSA-01/2016-17). K.W. and T.T. acknowledge support from the JSPS KAKENHI (Grant Numbers 21H05233 and 23H02052) and World Premier International Research Center Initiative (WPI), MEXT, Japan. G.J.S. thanks Condensed Matter Theory Center and Joint Quantum Institute, University of Maryland College Park, for their hospitality during the preparation of this manuscript. Y.G. acknowledges the support by the Deutsche Forschungsgemeinschaft (DFG) through grant No. MI 658/10-2 and RO 2247/11-1, the US-Israel Binational Science Foundation 2022391, and the Minerva Foundation. Y.G. is the incumbent of the InfoSys chair at IISc.

Author contributions

S.K., T.C., K.R.A., D.S., and A.B. conceived the idea of the study, conducted the measurements, and analyzed the results. T.T. and K.W. provided the hBN crystals. U.G., G.J.S., and Y.G. developed the theoretical model. All the authors contributed to preparing the manuscript.

Competing interests

The authors declare no competing interests.

Additional information

Supplementary information The online version contains supplementary material available at <https://doi.org/10.1038/s41467-024-52927-w>.

Correspondence and requests for materials should be addressed to Aveek Bid.

Peer review information *Nature Communications* thanks the anonymous, reviewer(s) for their contribution to the peer review of this work. A peer review file is available.

Reprints and permissions information is available at <http://www.nature.com/reprints>

Publisher's note Springer Nature remains neutral with regard to jurisdictional claims in published maps and institutional affiliations.

Open Access This article is licensed under a Creative Commons Attribution-NonCommercial-NoDerivatives 4.0 International License, which permits any non-commercial use, sharing, distribution and reproduction in any medium or format, as long as you give appropriate credit to the original author(s) and the source, provide a link to the Creative Commons licence, and indicate if you modified the licensed material. You do not have permission under this licence to share adapted material derived from this article or parts of it. The images or other third party material in this article are included in the article's Creative Commons licence, unless indicated otherwise in a credit line to the material. If material is not included in the article's Creative Commons licence and your intended use is not permitted by statutory regulation or exceeds the permitted use, you will need to obtain permission directly from the copyright holder. To view a copy of this licence, visit <http://creativecommons.org/licenses/by-nc-nd/4.0/>.

© The Author(s) 2024